Synthesis of α-Fluoro-α,β-unsaturated esters monitored by 1D and 2D benchtop NMR Spectroscopy

Dennis Weidener, Kawarpal Singh and Bernhard Blümich

Institut für Technische und Makromolekulare Chemie, RWTH Aachen University, Worringerweg 2, D-52074 Aachen, Germany

Abstract

For optimization and control of pharmaceutically and industrially important reactions chemical information is required in real time. Instrument size, handling and operation costs are important criteria to be considered when choosing a suitable analytical method apart from sensitivity and resolution. This present study explores the use of a robust and compact NMR spectrometer to monitor the stereo-selective formation of α-fluoro-α,β-unsaturated esters from α-fluoro-β-keto esters via deprotonation and deacylation in real-time. These compounds are precursors of various pharmaceutically active substances. The real-time study revealed the deprotonation and deacylation steps of the reaction. The reaction was studied at temperatures ranging from 293 to 333 K by interleaved 1D ^{1}H, ^{19}F and 2D ^{1}H-^{1}H COSY experiments. The kinetic rate constants were evaluated using a pseudo-first order kinetic model. The activation energies for the deprotonation and deacylation steps were determined to (-28 ± 2) and (63.5 ± 8) kJ/mol, respectively. This showed that the deprotonation step is fast compared to the deacylation step and that the deacylation step determines the rate of the overall reaction. The reaction was repeated three times at 293 K to monitor the repeatability and stability of the system. The compact NMR spectrometer provided detailed information on the mechanism and kinetics of the reaction which is essential for optimizing the synthetic routes for stepwise syntheses of pharmaceutically active substances.

Keywords: Reaction monitoring, Flow NMR, Compact NMR spectrometer, Deacylation, Deprotonation

This article has been accepted for publication and undergone full peer review but has not been through the copyediting, typesetting, pagination and proofreading process which may lead to differences between this version and the Version of Record. Please cite this article as doi: 10.1002/mrc.4843

1. Introduction

For understanding, optimization and cost reduction of chemical processes in industry and research it is important to understand their reaction mechanisms and kinetics. Different spectroscopic and chromatographic analytical tools are used for reaction monitoring and quality control such as Raman and ultraviolet spectroscopy [1,2], near Infrared (NIR) [3, 4] and Fourier transform infrared (FT-IR) spectroscopy [5], gas chromatography (GC) [6], high performance liquid chromatography (HPLC) [7], and more. Every technique provides specific information depending upon its sensitivity, resolution, stability and ability to probe into the chemical environment.

Nuclear magnetic resonance (NMR) spectroscopy has been used as an analytical instrument for reaction monitoring, process control and structure elucidation to obtain information about the various chemical groups involved in the reaction [8-9]. High-resolution NMR spectroscopy at high-field provides quantitative and qualitative information for monitoring chemical reactions and processes without prior calibration. But high-field NMR instruments are large and require cryogenic cooling gases, sophisticated laboratories, and experienced professionals for their maintenance and operation. On the other hand current state-of-the-art high-resolution compact NMR spectrometers have opened new possibilities for monitoring chemical processes at the production sites and at the chemical workbench [10-11]. These instruments are maintenance free and cost one-tenth of a high-field instrument.

The low-field compact NMR spectrometer used in this study operates with a Halbach magnet at a field strength of 1 Tesla corresponding to a ^{1}H NMR frequency of 42.5 MHz and a ^{19}F NMR frequency of 40.1 MHz. The magnet and the spectrometer are incorporated in one console of approximate size 40 $\times$ 70 $\times$ 50 cm^3 [12]. The magnetic field strength of the instrument is low compared to that of high-field spectrometers whose proton resonance frequencies go up to 1 GHz. In spite of this, the sensitivity and resolution of compact NMR spectrometers are sufficient to analyze a wide range of chemical reactions [13-14] and to elucidate the structures of small complex molecules [15]. Deuterated solvents are not required for the field frequency lock as the lock is external to the sample bore. The helps to avoid any potential kinetic isotope effects in the reaction which directly affect the reaction rate and activation energy. Moreover, shorter feed lines help to transport the reaction

mixtures in less time through the magnet than needed for high-field spectrometers which require long feed lines. Different reaction conditions can easily be realized, and experiments can be performed with a click of mouse button.

α-fluoro-α,β-unsaturated esters are used as precursors to many biologically important compounds in the syntheses of medicines, pheromones and herbicides [16]. The Wittig, Thia-Wittig and Julia olefinations are the main approaches used for synthesizing these compounds [17]. These approaches require expensive metal catalyst and starting materials, their selectivity is low, and the reaction conditions are harsh. But a new method has emerged to obtain the required product with high selectivity and with inexpensive reaction materials [18].

In the present work the kinetics and the percentage yield of the reaction were studied in real-time with a compact 1 T NMR spectrometer at temperatures varying from 293 to 333 K by interleaving 1D ^{1}H and ^{19}F and with 2D ^{1}H-^{1}H COSY experiments. The results obtained from the different experimental approaches are compared to assess the accuracy and versatility of the method. Because the reaction time was long, of the order of hours, one experiment was repeated three times to assess the repeatability of the reaction and the stability of the spectrometer.

2. Materials and Methods

Ethyl benzoyl acetate, selectfluor, benzaldehyde, cesium carbonate, sodium sulfate, sodium hydrogen carbonate, acetonitrile, ethyl acetate, hexane and silica gel 60 were purchased from Sigma Aldrich Chemie GmbH, Steinheim, and Alfa Aesar, Thermo Fisher (Kandel) GmbH, Karlsruhe, Germany.

3. Experimental

3.1 Synthesis of ethyl 2-fluoro-3-oxo-3-phenylpropanoate

Selectfluor ® (1 eq., 42.3 mmol, 15.0 g) was added portion wise to a solution of ethyl benzoyl acetate (1 eq., 42.3 mmol, 8.14 g) in 40 mL MeCN, at 293 K, and the resulting solution was stirred for two hours. The complete conversion of the starting materials was monitored using thin layer chromatography (TLC). The reaction mixture was diluted with dicholoromethane (DCM) (40 mL) to separate the organic and aqueous layers. The resulting organic layer was washed two times with saturated sodium bicarbonate (sat. $NaHCO_3$) solution. After separation, the organic

layer was dried over sodium sulphate ($NaSO_4$) and the solvent was removed under vacuum. The resulting yellow oil was purified with column chromatography (ethyl acetate: hexane, 1:1) yielding a colorless oil. 1D ^{1}H NMR spectra of the resultant product were measured at 9.4 and 1 Tesla. They showed the peaks of the phenyl group at around 7 ppm, the proton at the fluorinated position at 5.64 ppm and the signals corresponding to the CH_2 and CH_3 groups of the ethyl ester at 3.63 and 0.57 ppm.

^{1}H NMR (400 MHz, $CDCl_3$): δ = 7.61 – 6.98 (m, 5H), 5.64 (d, *J* = 47.7 Hz, 1H), 3.63 (q, *J* = 7.1 Hz, 2H), 0.57 (t, *J* = 7.0 Hz, 3H) ppm.
^{1}H NMR (43 MHz, $CDCl_3$): δ = 8.51 – 7.25 (m, 5H), 5.93 (d, *J* = 48.7 Hz, 1H), 4.28 (q, *J* = 7.2 Hz, 2H), 1.22 (t, *J* = 7.1 Hz, 3H) ppm.

3.2 Synthesis of ethyl (Z)-2-fluoro-3-phenylacrylate

A solution of benzaldehyde and ethyl 2-fluoro-3-oxo-3-phenylpropanoate in MeCN (9 mL) was placed inside a 100 ml reactor. Cesium carbonate (Cs_2CO_3) was added to the resultant mixture under constant stirring at 200 rpm to avoid mass transfer limitations due to inappropriate mixing. The temperature of the reaction was varied accordingly. After completion of the reaction, the reaction mixture was filtered, and the solvent was removed by rotary evaporation to obtain the raw product. The residue was purified by column chromatography on silica gel (ethyl acetate: hexane, 2:1) yielding the pure product. NMR spectra of the product were acquired at 9.4 and 1 Tesla, showing the magnetically different chemical groups.

^{1}H NMR (400 MHz, $CDCl_3$): δ = 7.63 (d, *J* = 6.9 Hz, 2H), 7.43 – 7.35 (m, 3H), 6.91 (d, *J* = 35.0 Hz, 1H), 4.34 (q, *J* = 7.1 Hz, 2H), 1.38 (t, *J* = 7.1 Hz, 3H) ppm.
^{1}H NMR (43 MHz, $CDCl_3$): δ = 7.81 – 6.45 (m, 5H), 6.03 (s, 1H), 3.77 (q, *J* = 6.9 Hz, 2H), 0.79 (t, *J* = 7.1 Hz, 3H) ppm.

3.3 Online monitoring procedure for real-time monitoring

A compact Magritek SpinSolve 1 T NMR spectrometer (Fig. 1) was employed for studying the reaction mechanism, kinetics and activation energy in real-time in the temperature range from 293 to 333 K.

3.3.1 Flow NMR setup and temperature

Each reaction was monitored by passing the mixture, from the round bottomed flask through the flow cell inserted in the bore of the NMR magnet with the aid of the three-channel peristaltic pump (ISMATEC® Relgo) at a flow rate of 1 ml/min. The flow cell with 4 mm inner diameter near the sensitive region of the NMR magnet and 1 mm inner diameter at the other regions away from the sensitive region was connected to polytetrafluoroethylene (PTFE) tubing forming a closed loop (Fig. 1a). A stainless steel filter was attached to the PTFE tubing to filter the reaction mixture before entering into the tubing. Each reaction was performed at the required temperature inside the round bottomed flask placed outside the NMR spectrometer. A mechanical stirrer was inserted on the top hole of the flask to agitate the mixture at the desired stirring speed. The reaction mixture was transferred to the NMR spectrometer at the temperature of the magnet by cooling down the reaction mixture by means of a cold-water bath placed between the reactor and the magnet. The reaction kinetics was assumed to be hardly affected because the reaction time was long between 6 to 24 hours compared to the transfer time of a few seconds. The temperature fluctuation inside the reactor was 0.9 K due to heat exchange with the surroundings. The PTFE tubing and flow cell were rinsed three times with methanol, water and acetone before each new use to remove any reaction residual adsorbed on the walls.

3.3.2 Delay times

Different characteristic times need to be considered to find the optimum flow rate for studying the reaction kinetics. The time difference between a change in the reaction mixture and the corresponding change in the signal amplitude of the reaction mixture depends on the different characteristic times encountered in the flow setup [19-20]. The transfer time t_{trans}, delay time t_{delay}, dwell time t_{dwell} and residence-time-distribution (RTD) curves for the same setup are discussed elsewhere [21-24].

3.3.4 Data acquisition

Each 1D ^{1}H NMR spectrum at 1 T was acquired with single scan using a π/2 excitation pulse of 7 μs, an acquisition time of 6.6 s, an acquisition bandwidth of 5 kHz and a dwell time of 200 μs with 32 768 data points. Each 1D ^{19}F NMR spectrum was obtained with 4 scans. Every scan was recorded using a π/2

excitation pulse of 27 µs, an acquisition bandwidth of 20 kHz, an acquisition time of 1.6 s and a dwell time of 50 µs with 32 768 data points. The delay before each 1D ^{1}H and 2D ^{1}H-^{1}H COSY was 15 seconds and before each ^{19}F scan was 10 seconds. The delays were optimized to be in quantitative mode. Each 2D ^{1}H-^{1}H COSY spectrum was obtained in 9 minutes using 256 t_1 increments and one scan. The 1D ^{1}H NMR spectra at 9.4 T were measured in 1.5 minutes with a Bruker (AVANCE III) spectrometer using a 30° pulse flip angle and 16 scans. The data were processed with automatic phase and baseline corrections.

3.3.5 Processing of the low-field data

The FIDs were recorded and saved by the SpinSolve (Magritek GmbH, Aachen) software. They were processed and analyzed using the MestreNova (Version 11.0, Mestrelab Research S. L., Santiago de Compostela, Spain) software. Exponential windowing of 0.6 Hz was applied to increase the sensitivity of the spectra. The baseline of each spectrum was corrected with a zero-order polynomial. Both the 1D ^{1}H and ^{19}F spectra were processed with same processing parameters. The peaks of interest were integrated to obtain the variation in signal amplitude as a function of time. The integration ranges were selected depending upon line width and peak overlap. The derived values were exported to the Origin (version 9.0, OriginLab, Northampton, MA) for plotting. The values of the rate constants were evaluated by fitting a kinetic model to the signal-amplitude vs. time curves. The activation energy graphs were plotted in Origin with the obtained rate constants.

4. Results and discussion

4.1 Reaction scheme and mechanism

The reaction of ethyl 2-fluoro-3-oxo-3-phenylpropanoate (**A**) with benzaldhyde (**B**) in the presence of cesium carbonate leads to the formation of ethyl (Z)-2-fluoro-3-phenylacrylate (**C**) along with benzoic acid (**D**) as a side product (reaction scheme). The reaction consists of three steps (Fig. 2). The first step involves the deprotonation of α acetic proton present at the fluorinated position of ethyl 2-fluoro-3-oxo-3-phenylpropanoate (**A**) with cesium carbonate acting as a base. The second step involves the coupling of the deprotonated compound (**I**) with benzaldehyde (**B**). The

third step involves a rearrangement of bonds between species (**II**) and (**III**) with simultaneous formation of a double bond at the fluorinated site along with the elimination of benzoic acid (**D**) and formation of the product ethyl (Z)-2-fluoro-3-phenylacrylate (**C**) [17]. The deprotonation step 1 and the formation of the final product ethyl (Z)-2-fluoro-3-phenylacrylate (**C**) in step 3 were monitored with the compact NMR spectrometer in real time. The lifetime of the intermediate involving elimination and bond formation was very short compared to the NMR measurement time, therefore, it cannot be observed with NMR. The formation of the short-lived intermediate in the deacylation step is the rate determining step of the reaction which is responsible for the final outcome of the reaction.

4.2 1D NMR spectroscopy

The NMR spectra of the starting materials were recorded in acetonitrile (MeCN) at the same concentrations as those used for real-time monitoring. The 1D ^{1}H NMR spectrum of ethyl 2-fluoro-3-oxo-3-phenylpropanoate (**A**) (Fig. 3a) showed a triplet at 0.8 ppm from the (CH_3-) group, a quartet centered at 3.8 ppm from the (-CH_2-) group of the (-CH_2-CH_3) ethyl group. The doublet centered at 5.8 ppm arises from the coupling of fluorine with proton through ^{2}J coupling with a large coupling constant of 47.5 Hz. The superimposed multiplet centered at 7 ppm arises from aromatic ring. The 1D ^{1}H NMR spectrum of benzaldehyde (**B)** (Fig. 3b) showed a single peak from the benzaldehyde proton at 9.6 ppm. The multiplet centered at 7 ppm arises from the aromatic ring. The 1D ^{1}H NMR spectra of the mixture of both compounds (**A+B**) before (Fig. 3c) and after catalyst addition (Fig. 3d) show the impact of the deprotonation reaction of compound **A** with the base cesium carbonate. The doublet present in the Fig. 3c is not present in Fig. 3d because of the loss of the proton from the fluorinated site. The 1D ^{1}H NMR spectrum of the reaction mixture (Fig. 3e) contains mainly the unreacted benzaldehyde (**B**) and ethyl (Z)-2-fluoro-3-phenylacrylate (**C**) (product) and benzoic acid (**D**) obtained at the end of the reaction after 22 hours. The spectrum shows a single peak from the double bond proton at 6.1 ppm. The deprotonation causes the compound to precipitate due to low solubility, leaving no signal of the starting material (**A**) in the NMR spectrum. The 1D ^{19}F NMR spectra of the starting material (**A)** and the product (**C)** both showed one doublet centered at -189.3 ppm and -124.7 ppm, respectively [25].

4.3 2D NMR spectroscopy

The reaction was also monitored at 293 K by 2D ^{1}H-^{1}H COSY NMR spectroscopy. Because the reaction was very slow, the time-dependent concentration changes could also be observed by 2D NMR spectroscopy during the course of the reaction. The 2D ^{1}H-^{1}H COSY NMR spectrum (Fig. S1) of the reaction mixture observed after 22 hours showed excellent signals from the ^{3}J coupling between the CH_2 and CH_3 groups of the ester group. These off-diagonal peaks were used to monitor the progress of the reaction because they vanish after the catalyst addition due to precipitation and again appear with the formation of the product.

4.4 Online monitoring of the reaction

The reaction was monitored in real-time by interleaved 1D ^{1}H-^{19}F NMR spectroscopy. The 3D stack plot of the ^{1}H NMR spectra (Fig. 4) obtained as a function of time shows the change in the concentrations of the different chemical groups involved in the reaction. The change in the signal amplitudes was used to determine the reaction kinetics. The signal intensity of the single peak from the benzaldehyde (**B**) proton at 9.6 ppm decreases, whereas a singlet at 6.1 ppm from the double bond proton and the quartet at 3.8 ppm from the -CH_2 group of ethyl (Z)-2-fluoro-3-phenylacrylate (**C**) increase with time. The multiplet observed in the aromatic region from 6.5 to 8 ppm changes its shape from start to end of the reaction. The maximum of the multiplet at the beginning of the reaction is at higher chemical shifts and decreases over time. This shows the absence of the more shielding carbonyl group present in the reactant (**A**) which deshields the protons via resonance leading to higher chemical shifts of the proton. Simultaneously a new maximum in the aromatic region of the product (**C**) arises at lower chemicals shift.

4.5 Evaluation of Reaction Kinetics

The reaction kinetics were evaluated from fitting the signal amplitude-time plots with the kinetic model. The reaction consists of two main steps. The first deprotonation step consists of the reaction of ethyl 2-fluoro-3-oxo-3-phenylpropanoate (**A**) with the cesium carbonate catalyst. It is followed by the deacylation step consisting of the reaction of the deprotonated reactant (**A)** and benzaldehyde (**B**).

The first deprotonation step was very fast compared to second deacylation step. Even at the lowest temperature of 293 K, the deprotonation time was 4 minutes compared to the deacylation which was 22.5 hours. This suggests that the deprotonation step has no influence on the second reaction step. Therefore, both steps were assumed to be separate reaction steps and the rate constants and activation energies of both steps were calculated independently.

The deprotonation step proceeds with first order kinetics because the concentration of the catalyst does not vary with time. The kinetic expression obtained for the deprotonation steps becomes,

$$[\mathrm{A}] = [\mathrm{A}]_0 \cdot \mathrm{e}^{-kt}. \quad (1)$$

Here, *k* is the rate constant of the reaction. [A] and $[A]_0$ are the concentrations of ethyl 2-fluoro-3-oxo-3-phenylpropanoate (**A**) at times *t* and 0, respectively. Equation (1) was fitted to the signal amplitude-time plot (Fig. 5a) of the first step to obtain the kinetic rate constant. The plot of the residuals illustrates the good quality of the fit (Fig. 5b).

The deprotonated compound (**I**) precipitates and its concentration diminishes relative to that of the other reactant benzaldehyde (**B**) so that the reaction becomes pseudo-first order. Therefore, the rate of change of benzaldehyde (**B**) determines the kinetics of the reaction.

The deprotonation step proceeds with first order kinetics because the concentration of catalyst does not vary with time. The kinetic expression obtained for the deprotonation steps becomes,

$$[\mathrm{B}] = [\mathrm{B}]_0 \cdot \mathrm{e}^{-kt}. \quad (2)$$

Here, *k* is the rate constant of the reaction. [B] and $[B]_0$ are the concentrations of benzaldehyde (**B**) at time *t* and 0, respectively. Equation (2) was fitted to the signal amplitude-time plot (Fig. 6a) of first step to obtain the kinetic rate constant. The plot of the residuals shows the good quality of the fit (Fig. 6b).

4.6 Repeatability measurements

The instrument stability is essential for obtaining good quantitative and qualitative results. Three experiments were carried out with same initial reaction conditions at

293 K with real-time monitoring by 1D ^{1}H, ^{19}F and 2D ^{1}H-^{1}H COSY NMR spectroscopy in the interleaved mode. Each series of ^{1}H-^{19}F-(^{1}H-^{1}H-COSY) experiments took 10 minutes. Therefore, 6 points were monitored with each method in one hour. This time resolution was sufficient to monitor the reaction with more 22 hours reaction time. As The peaks used for integration were quite distinct from the overlapping peaks, so that the effect of changing integration limit on the repeatability was not considered. The same integration limits were used for every reaction to check the repeatability. The reaction showed excellent repeatability and stability which is manifested by the ^{1}H NMR spectra (Fig. 7a) but also by the ^{19}F spectra (Fig. S2). The 2D ^{1}H-^{1}H experiments showed comparatively poor repeatability compared to the ^{1}H and ^{19}F due to the long experiment time of 9 min during which changes in the component concentrations affect the quantification more strongly than in the 1D ^{1}H and ^{19}F experiments. Also, the signal-to-noise ratio of 2D experiments was less compared to the 1D experiments leading to differences in the rate constants and repeatability obtained from the 2D experiment. However, the 2D experiments can serve as a tool to understand the coupling interactions of various chemical groups. The reaction rate constants obtained with 1D ^{1}H and ^{19}F were within the error range and have a low coefficient of variation (Tab. 1). The integration of the whole spectrum showed excellent field stability and mass balance during the total reaction time of more than 22 hours (Fig. 7a).

4.7 Effect of temperature on the reaction rate

The reaction was performed at different temperatures ranging from 293 to 333 K to determine the impact of temperature on the reaction rate using the stoichiometric concentration (Fig. 7b). The variation in signal amplitude of the benzaldehyde (**B**) proton showed faster conversion of benzaldehyde to product at higher temperatures than at lower temperatures. The rate constants (Tab. 2) of each reaction step were evaluated by fitting the kinetic equations (1) and (2) to the data obtained with ^{1}H NMR spectroscopy.

The percentage yield for each reaction was calculated from the spectral data and is within the range of literature values [18]. The determined values of the rate constants are within the standard range for reactions in solution, which can also be appreciated after calculating the Q_{10} factor which describes the change of the reaction rate for a temperature change of 10 K. The averaged Q_{10} factor for the

deacylation calculated from the proton measurements is Q_{10} = 2.7 which is in the range for reactions performed in solution.

Arrhenius plots were obtained for the separate deprotonation and deacylation steps of the reaction using the rate constants obtained from fitting the kinetic model. The activation energy of each step was calculated from the slope of the Arrhenius plots. A negative activation energy of (-28 ± 2) kJ/mol was calculated for the deprotonation step (Fig. 8a) while a positive activation energy of (63.5 ± 8.3) kJ/mol was evaluated for the deacylation step (Fig. 8b). This suggests that the deprotonation step is very fast compared to the deacylation step confirming that the deacylation is the rate determining step of the reaction.

5 Conclusion

The synthesis of α-fluoro- α β-keto unsaturated esters was monitored in real-time by NMR with a tabletop 1 T spectrometer. A series of interleaved ^{1}H-^{19}F-(^{1}H-^{1}H 2D COSY) experiments was executed to study the mechanistic details and kinetics at different temperatures under stoichiometric conditions. The deprotonation step is difficult to monitor in batch and inline modes because of the required time resolution. The deprotonation step is very fast compared to the deacylation step. The compact NMR spectrometer provides sufficient sensitivity and resolution to monitor the reaction under the given reaction conditions at low concentrations and without deuterated solvents. The longest experiment of 22 hours was repeatedly monitored by interleaved experiments to assess the repeatability and stability of the system. The results obtained show excellent agreement between ^{1}H, ^{19}F and 2D ^{1}H-^{1}H COSY spectroscopy as different reaction monitoring methods. The activation energies of the deprotonation and deacylation steps were obtained separately. The activation energy of the deprotonation step was obtained to be (-28 ± 2) kJ/mol and for the deacylation steps was (63.5 ± 8) kJ/mol. This shows that the deacylation step is the rate determining step of the reaction while the deprotonation step is very fast. Furthermore, the rate constants obtained from the deprotonation reaction are one order of magnitude higher than those for the diacylation reaction. A negative activation energy emerges from the exothermic solubility behavior of the cesium carbonate reactant in the deprotonation step. NMR spectroscopy with a compact instrument has the potential to explore not only the kinetics of the various reaction

components but also the mechanistic details and the behavior of different components during the various steps of the reaction.

Conflict of interest

BB is on the board of directors of Magritek.

Acknowledgements

The authors gratefully acknowledge financial support from DFG Gerätezentrum Pro2NMR, a DFG supported joint instrumental NMR facility of RWTH Aachen University and KIT Karlsruhe.

References

1. J. B. Cooper, *Chemometr. Intell. Lab. Syst*. **1999**, *46*, 231.
2. J. van den Broeke, G. Langergraber, *Spectroscopy Europe* **2006**, *18*, 15.
3. T. De Beer, A. Burggraeve, M. Fonteyne, L. Saerens, J. P. Remon, C. Vervaet, *Int. J. Pharm*. **2011**, *417*, 32.
4. G. Knothe, *J. Am. Oil Chem. Soc*. **2000**, *77*, 489.
5. N. Doki, H. Seki, K. Takano, H. Asatani, M. Yokota, N. Kubota, *Cryst. Growth Des*. **2004**, *4*, 949.
6. G. Guiochon, C.L. Guillemin, *Quantitative gas chromatography for laboratory analyses and on-line process control*, Elsevier, 1988.
7. L. Zhu, R.G. Brereton, D.R. Thompson, P.L. Hopkins, R.E. Escott, *Anal. Chim. Acta* **2007**, *584*, 370.
8. H. Friebolin, *Basic One- and Two-Dimensional NMR Spectroscopy*, 5th ed., Wiley-VCH, Weinheim, 2011.
9. H. Günther, *NMR Spectroscopy: Basic Principles, Concepts, and Applications in Chemistry*, 3rd ed., Wiley-VCH, Weinheim, 2013.
10. K. Singh, B. Blümich, *Trends Anal. Chem*. **2016**, *83*, 12.
11. B. Blümich and K. Singh, *Angew. Chem*. **2018**, *57*, 6996.
12. B. Blümich, S. Haber-Pohlmeier, W. Zia, *Compact NMR*, de Gruyter, Berlin, 2011.
13. E. Danieli, J. Perlo, A. Duchateau, G. Verzijl, V. Litvinov, B. Blümich, F. Casanova, *ChemPhysChem* **2014**, *15*, 3060.
14. M. Killner, Y.G. Linck, E. Danieli, J. Rohwedder, *Fuel* **2015**, *139*, 240.

15. K. Singh, B. Blümich, *Analyst* **2017**, *142*, 1459.
16. B. Davies, F. Maesen, C. Baur, *Ciprofloxacin*, Springer, 1986, pp. 97-102.
17. D.B. Longley, D.P. Harkin, P.G. Johnston, *Nat. Rev. Cancer* **2003**, *3*, 330.
18. J. Qian, W. Yi, M. Lv, C. Cai, *Synlett*. **2015**, *26*, 127.
19. N. Zientek, C. Laurain, K. Meyer, M. Kraume, G. Guthausen, M. Maiwald, *J. Magn. Reson*. **2014**, *249*, 53.
20. F. Dalitz, L. Kreckel, M. Maiwald, G. Guthausen, *App. Magn. Reson*. **2014**, *45* 411.
21. K. Singh, B. Blümich, *Analyst* **2018**, *143*, 4408.
22. M. Maiwald, H. H. Fischer, Y. K. Kim, K. Albert, H. Hasse, *J. Magn. Reson*. **2004**, *166*, 135.
23. M. V. S. Elipe, R. R. Milburn, *Magn. Reson. Chem*. **2016**, *54*, 437.
24. F. Dalitz, M. Maiwald, G. Guthausen, *Chem. Eng. Sci*. **2012**, *75*, 318.
25. V. Sans, L. Porwol, V. Dragone, L. Cronin, *Chem. Sci*. **2015**, *6*, 1258.

Table 1. Rate constants obtained for the deacylation reaction step repeated three times using three measurement methods at 293 K.

Method	$k \times 10^5$ [s^{-1}]	$k \times 10^5$ [s^{-1}]	$k \times 10^5$ [s^{-1}]	Coefficient of variation [%]
^{1}H	4.74 ± 0.08	4.73 ± 0.07	4.59 ± 0.08	1.8
^{19}F	4.28 ± 0.26	4.05 ± 0.66	4.61 ± 0.55	6.5
COSY	3.98 ± 0.29	4.21 ± 0.36	2.94 ± 0.40	18

Table 2. Rate constants for both reaction steps at temperatures ranging from 293 K to 333 K.

S. No.	Temperature [K]	$k_{Deprot.} \times 10^2$ [s^{-1}]	$k_{deacyl} \times 10^4$ [s^{-1}]	Yield [%]
1	293	2.36 ± 0.19	0.47 ± 0.01	50.0
2	303	1.50 ± 0.39	1.23 ± 0.03	59.8
3	318	0.98 ± 0.17	3.52 ± 0.06	66.0
4	333	0.61 ± 0.69	8.71 ± 0.24	72.5

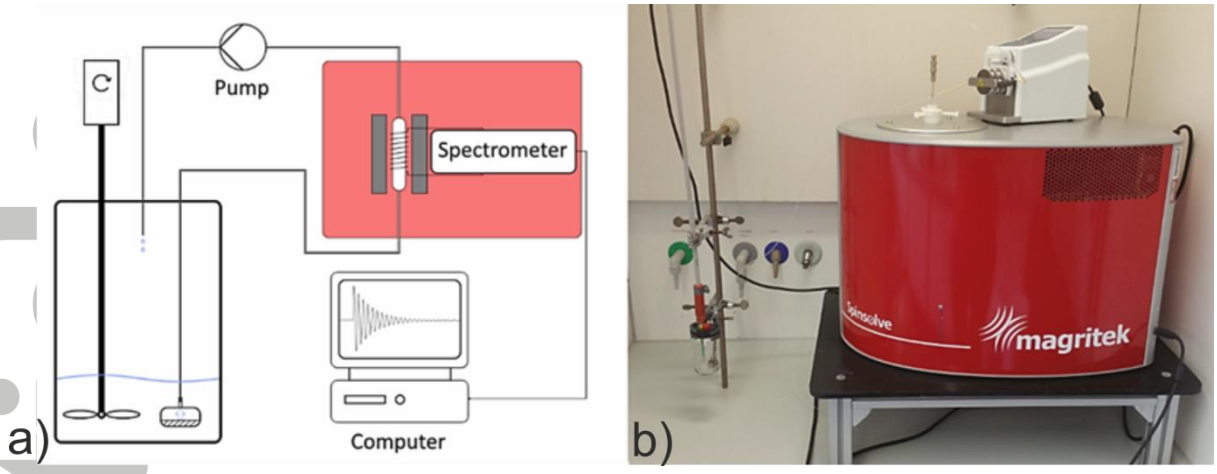

Figure 1: a) Real-time reaction monitoring scheme. b) Compact Magritek 1 T NMR spectrometer

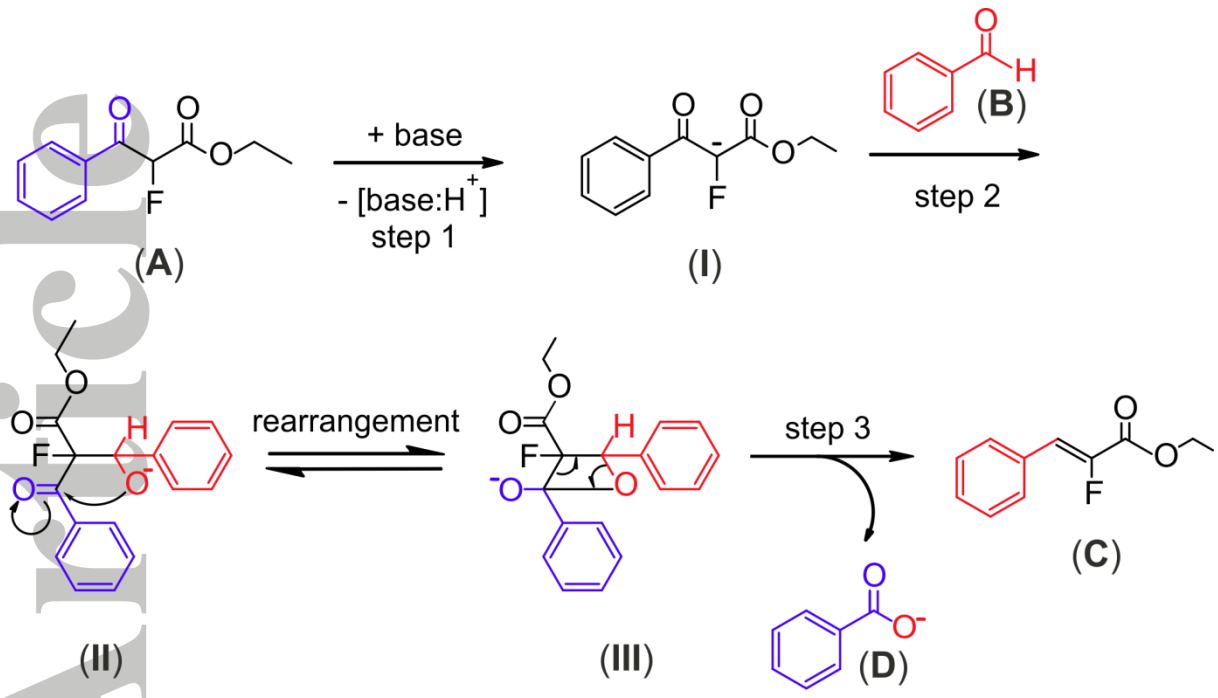

Figure 2: Mechanism of the reaction.

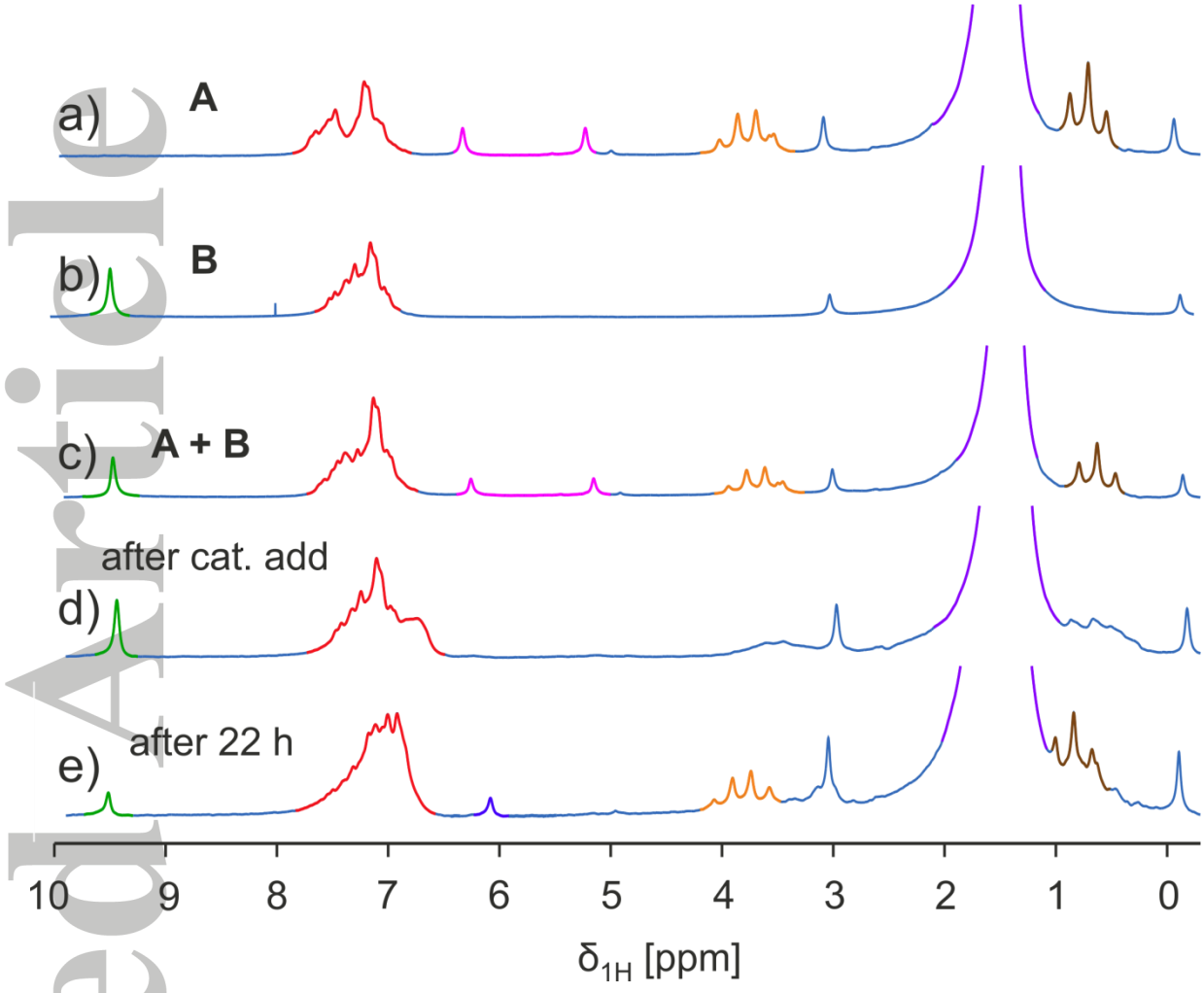

Figure 3: 1D 1H NMR spectra of the different compounds involved in the reaction. a) Ethyl 2-fluoro-3-oxo-3-phenylpropanoate (A). b) Benzaldehyde (B). c) Mixture of A and B. d) Mixture of (A), (B) and cesium carbonate catalyst. e) Reaction mixture containing benzaldehyde (B), ethyl (Z)-2-fluoro-3-phenylacrylate (C), benzoic acid (D) after 22 hours for the reaction performed at 293 K.

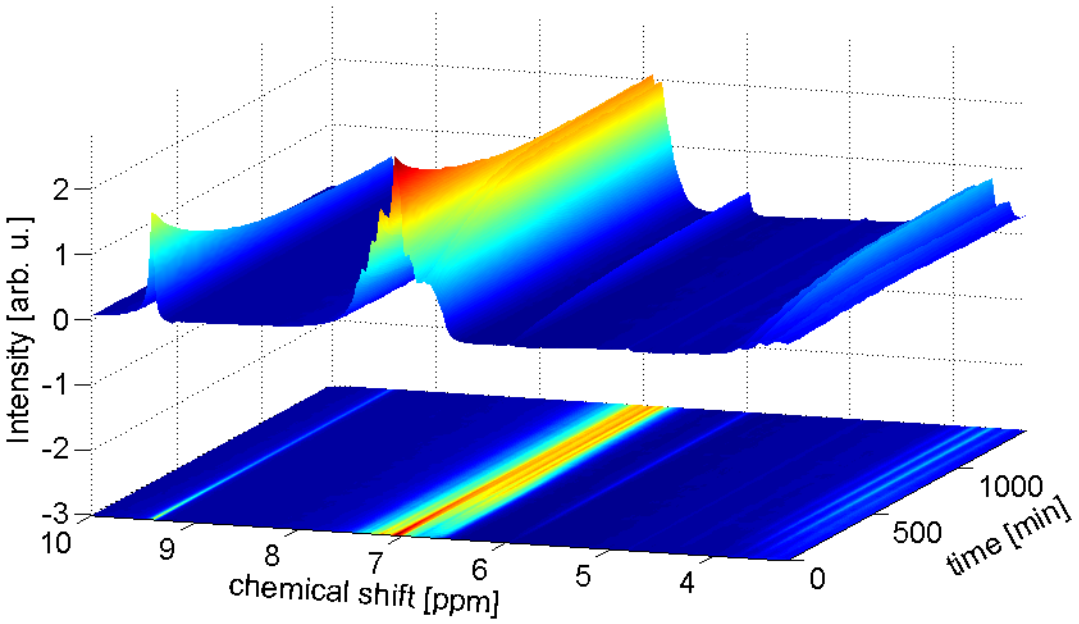

Figure 4: 3D stack plot (top) of 1D ^{1}H NMR spectra and its projection onto the x-y plane (bottom) for the reaction performed at 293 K.

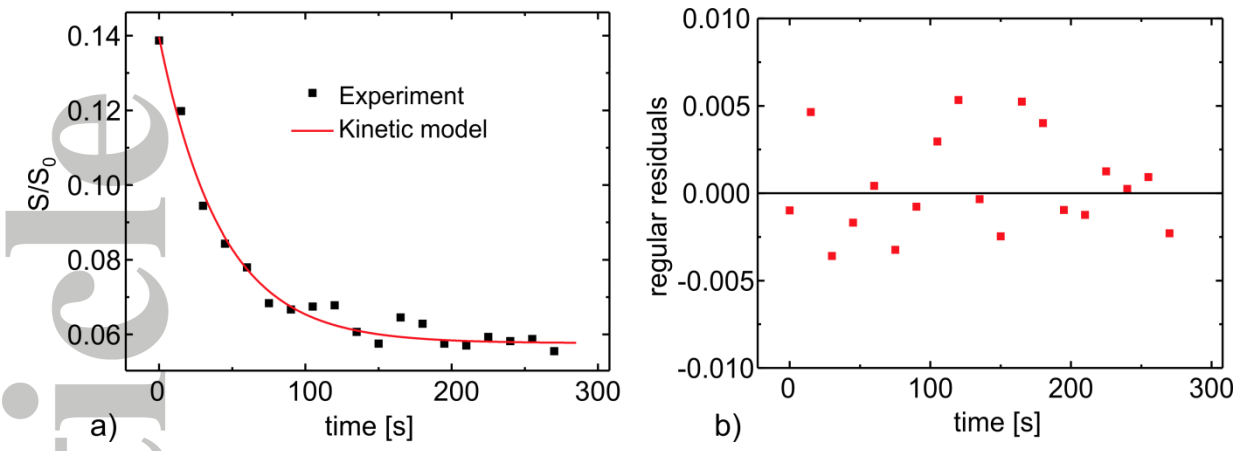

Figure 5. Kinetic model fitted to the experimental data obtained for the deprotonation reaction. a) Pseudofirst order kinetic model fitted to the signal amplitude-time plot of fluorinated proton of ethyl 2-fluoro-3-oxo-3-phenylpropanoate (A). b) Residuals of the fit.

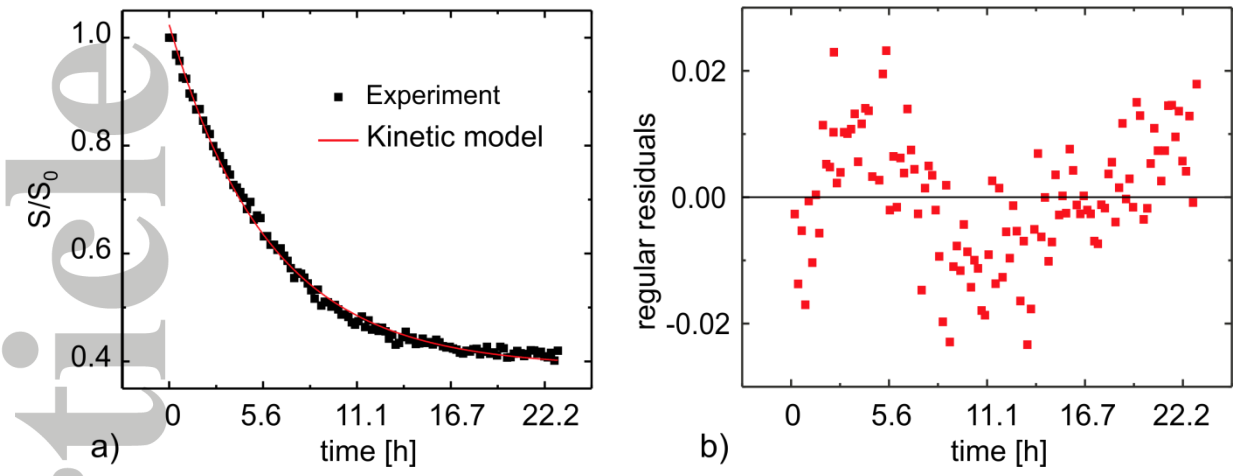

Figure 6. Kinetic model fitted to the experimental results obtained for the deacylation reaction. a) Pseudofirst order kinetic model fitted to the signal amplitude-time plot of benzaldehyde (B) proton. b) Residuals of the fit

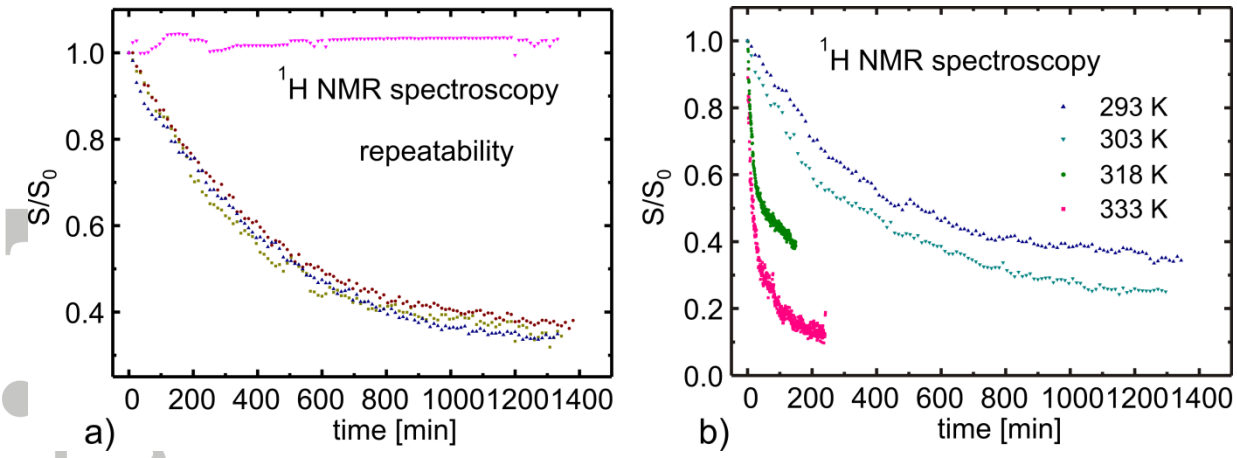

Figure 7: Variation of the signal amplitude of the aldehyde proton of benzaldehyde (B) with time from 1D ^{1}H NMR spectroscopy. a) At 293 K for three identical reactant concentrations along with mass balance. b) At temperatures ranging from 293 to 333 K.

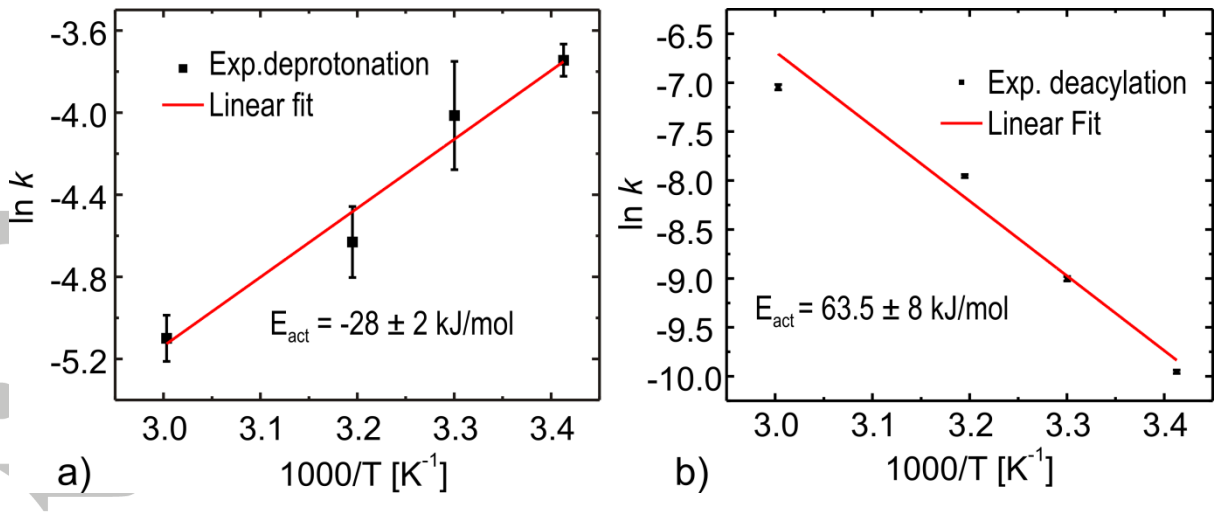

Figure 8: Arrhenius plots for both reaction steps. a) Deprotonation. b) Deacylation.

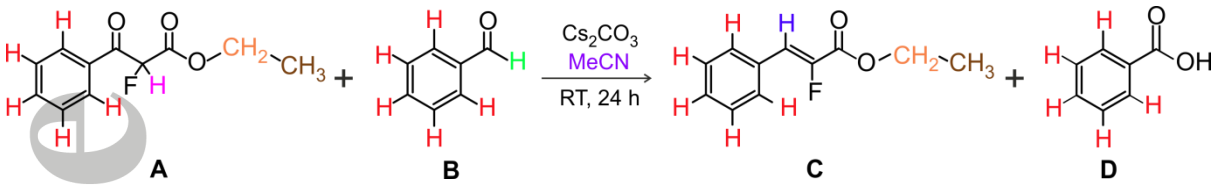

Scheme 1